Ulrich Stopper, Manfred Aigner, Holger Ax, Wolfgang Meier, Rajesh Sadanandan, Michael Stöhr, Alessio Bonaldo, PIV, 2D-LIF and 1D-Raman measurements of flow field, composition and temperature in premixed gas turbine flames, Experimental Thermal and Fluid Science 34 (2010) 396-403.

The original publication is available at www.elsevier.com

http://dx.doi.org/10.1016/j.expthermflusci.2009.10.012

PIV, 2D-LIF and 1D-Raman measurements of flow field, composition and temperature in premixed gas turbine flames

U. Stopper [a,*], M. Aigner [a], H. Ax [a], W. Meier [a], R. Sadanandan [a], M. Stöhr [a], A. Bonaldo [b]

[a] *German Aerospace Center (DLR), Institute of Combustion Technology, Pfaffenwaldring 38-40, D-70569 Stuttgart, Germany*
[b] *Siemens Industrial Turbomachinery Ltd., Combustion Group, P O Box 1, Waterside South, Lincoln LN5 7FD, UK*

A B S T R A C T

Several laser diagnostic measurement techniques have been applied to study the lean premixed natural gas/air flames of an industrial swirl burner. This was made possible by equipping the burner with an optical combustion chamber that was installed in the high pressure test rig facility at the DLR Institute of Combustion Technology in Stuttgart. The burner was operated with preheated air at various operating conditions with pressures up to $p = 6$ bar and a maximum thermal power of $P \approx 1$ MW.
The instantaneous planar flow field inside the combustor was studied with particle image velocimetry (PIV). Planar laser induced fluorescence (PLIF) of OH radicals on a single-shot basis was used to determine the shape and the location of the flame front as well as the spatial distribution of reaction products. 1D laser Raman spectroscopy was successfully applied for the measurement of the temperature and the concentration of major species under realistic gas turbine conditions.
Results of the flow field analysis show the shape and the size of the main flow regimes: the inflow region, the inner and the outer recirculation zone. The highly turbulent flow field of the inner shear layer is found to be dominated by small and medium sized vortices. High RMS fluctuations of the flow velocity in the exhaust gas indicate the existence of a rotating exhaust gas swirl. From the PLIF images it is seen that the primary reactions happened in the shear layers between inflow and the recirculation zones and that the appearance of the reaction zones changed with flame parameters. The results of the multiscalar Raman measurements show a strong variation of the local mixture fraction allowing conclusions to be drawn about the premix quality. Furthermore, mixing effects of unburnt fuel and air with fully reacted combustion products are studied giving insights into the processes of the turbulence-chemistry interaction.

Keywords:
Combustion
High pressure
Turbulence-chemistry interaction
Laser diagnostics
Velocity
Raman spectroscopy

Nomenclature

CFD Computational fluid dynamics

[*] Corresponding author. Tel.: +49 711 6862 357; fax: +49 711 6862 578.
E-mail address: ulrich.stopper@dlr.de

GT	Gas turbine
ICCD	Intensified charge-coupled device
IRZ	Inner recirculation zone
LIF	Laser induced fluorescence
OH*	Electronically excited OH
ORZ	Outer recirculation zone
PDF	Probability density function
PIV	Particle image velocimetry
PLIF	Planar LIF
RMS	Absolute standard deviation (root mean square)
SHG	Second-harmonic generation
YAG	Yttrium-aluminum-garnet

f	Focal length
P	Thermal power
p	Absolute pressure inside combustion chamber
Δp	Pressure drop over the burner
T	Gas temperature
X	Volume fraction
Φ	Equivalence ratio
ξ	Mixture fraction

1. Introduction

In modern stationary gas turbine (GT) combustors the concept of lean premixed combustion is mostly applied in order to achieve a homogenous temperature distribution at lean flame conditions. In this way, local temperature peaks are avoided and NO_x emissions are reduced. However, this concept is prone to combustion instabilities, especially in combination with commonly used swirl burners. Of particular practical relevance are thermo-acoustic instabilities which can arise from the interaction of the heat release rate, the flow field and the combustor geometry [1-5]. Further effects which limit the exploitation of the full potential of lean premixed combustion are unmixedness of fuel and air [6,7], unsteady flame stabilization [8] or hydrodynamic instabilities [9,10]. In general, GT-like flames are highly turbulent and exhibit strong effects of turbulence-chemistry interactions like ignition delay or local flame extinction [11-13]. Up to date there is still a lack in understanding these phenomena, and further experimental and numerical investigations are necessary.
Recently, detailed laser diagnostic studies in GT-relevant combustors have contributed to an improved understanding of the phenomena mentioned above. Frequently used measuring techniques were particle image velocimetry (PIV) or laser Doppler velocimetry (LDV) for the flow field, laser induced fluorescence (LIF) for flame radicals, tracers, pollutants or temperature, coherent anti-Stokes Raman scattering (CARS) for temperature, and laser Raman scattering for species concentrations [14]. In some research groups, high-pressure test rigs have been equipped with optical access in order to apply these techniques to GT combustion processes under realistic conditions, i.e. preheated air, high thermal loads, high turbulence levels and relevant combustor geometries, see for example [15-24].
In the investigations presented here, an industrial GT burner was equipped with an optical combustion chamber, installed in the high pressure test rig at the Institute of Combustion Technology of the German Aerospace Center (DLR) in Stuttgart and investigated using different laser diagnostic techniques. The combustor was operated with natural gas and preheated air and the operating conditions were varied in a wide range of thermal power,

equivalence ratio and pressure. Main goals of the study were a detailed characterization of the flow field and the combustion process, the quantification of the degree of mixing, the identification of effects of turbulence-chemistry interactions and the investigation of transient flame behavior. Planar LIF of OH and OH* chemiluminescence imaging were applied to determine the flame structures and the stabilization region, PIV was used for the measurement of the flow velocities and 1D-laser Raman scattering was used to quantitatively measure the major species concentrations (N_2, O_2, H_2O, C_xH_y, CO_4, CO and H_2) and the temperature. The Raman technique also enabled the determination of the local mixture fraction and the reaction progress, revealing effects of unmixedness and turbulence-chemistry interactions.
The foci of this paper lie on the demonstration of the potential of laser techniques for the investigation of GT flames under realistic conditions and on the experimental characterization of an industrial GT burner at elevated pressure. Not all details of the burner and operating conditions can be published because some details of the industrial burner are subject to confidentiality.

2. Experimental setup

2.1. Combustor and high-pressure test rig

The GT burner under investigation was a G30 DLE (Dry Low Emissions) burner manufactured by Siemens Industrial Turbomachinery in Lincoln, UK [25]. It is installed in the range of small industrial gas turbines from the SGT-100 at 5 MW to the SGT-400 at 13.4 MW. For optical and laser measurements it was equipped with an optically accessible combustion chamber (Fig. 1) which is capable of securely confining flames with a thermal power of up to 1 MW. This burner was operated at high mass flows and with preheated air in a high-pressure test rig. The inner dimensions of the square combustor resemble the size of the SGT-100 combustor. Cooling channels in the side walls reduced the thermal load of the quartz windows. The preheated air had a temperature of 400 °C and was guided through these channels before reaching the burner plenum. A water-cooled transition duct feeds the hot exhaust gas into the rig's exhaust channel. For the velocimetry measurements the flow had to be seeded with small particles (1 µm) of titanium dioxide. A perforated ring tube upstream of the swirler was used for their injection. All measurements were performed at pressures p between 1.5 and 6 bars and relative burner pressure drops $\Delta p/p$ between 1 % and 3 %.
This combustor was installed at the high-pressure test rig facility HBK-S of the Institute of Combustion Technology in Stuttgart. The pressure vessel housing the combustor also has quartz windows for the optical access accompanied by several probes for measuring temperature, absolute pressure, differential pressure, acoustics and exhaust gas composition.

<Figure 1>

2.2. Particle image velocimetry (PIV)

The diagnostic setup for the velocity measurements can be seen in Fig. 2. A flashlamp pumped frequency-doubled Nd:YAG laser (New Wave Solo PIV 120) was used for illuminating the PIV particles. The laser pulse energy was 120 mJ at a pulse duration of 5 ns. Before entering the combustion chamber, the laser beam was expanded into a light sheet using two cylindrical lenses (f_1 = -12.7 mm and f_2 = 200 mm) and a spherical lens (f = 1000 mm). With a double-pulse delay of 10-15 µs particle imaging was performed at a repetition rate of 5 Hz. A camera lens with f = 50 mm, f/5.6 and a narrow band filter (532 nm) in front of it depicted the PIV images onto a CCD chip (LaVision, 1376 × 1024 pixels).

The spatial resolution of the measured velocity depends on the seeding particle density, the degree of window contamination, and the turbulence of the flow. At good conditions, an interrogation window size of 12 × 12 pixels could be achieved. The accuracy of the single-shot velocity can reach ±0.7 m/s (assuming a subpixel accuracy of the particle displacement of 0.1 pixel and neglecting the influence of unrecognized erroneous vectors).
The ICCD camera with the filter shown in Fig. 2 was installed to provide images of the OH* chemiluminescence. It was used for observing the shape of the flame.

<Figure 2>

2.3. Planar laser-induced fluorescence (PLIF) of OH

A frequency-doubled dye laser (Lumonics HD-500, $\tau_{pulse} \approx 8$ ns, $E_{pulse} \approx 4.6 – 5.5$ mJ) pumped by a Nd:YAG laser (Quanta Ray, DCR-2) was used for the excitation of OH radicals. The light sheet for planar measurements was generated by one cylindrical (f = -50 mm) and one spherical lens (f = 750 mm). Before the laser beam reached the expansion optics, a small portion of the pulse energy was coupled out by a beam splitter (Fig. 3) and guided through the flat laminar flame of a matrix burner. The LIF emission from this flame was observed by a photo multiplier tube equipped with a spectral bandpass filter that is transparent for wavelengths between 300 nm and 325 nm. The signal of the photo multiplier was used as a reference for the adjustment of the laser wavelength. With this setup it was possible to tune the dye laser to 283.55 nm (output of the SHG crystal), which is resonant with the $Q_1(8)$ line of the A-X (1-0) band of the OH radical. A second beam splitter reflected a fraction of the laser sheet into a dye cell that was observed by an intensified CCD camera (Princeton Instruments PI-Max). The fluorescence distribution from the dye cell which is proportional to the intensity distribution of the laser sheet was recorded with this camera for every single shot. Such intensity profiles are essential for a proper processing of the raw data. The largest part of the pulse energy was irradiated into the combustor. Like the laser sheet of the PIV system, the PLIF laser sheet was always located in the central plane of the combustor. It was only moved along the axial direction in order to measure OH distributions in different sections of the combustor as the sheet was only about half as wide as the field of view. The detection of the LIF signal from the combustion chamber was done with a further ICCD camera (Princeton Instruments PI-Max, 512 × 512 pixels). An objective suitable for UV imaging (f = 100 mm, f/2) and a bandpass filter identical to the one in front of the photo multiplier were mounted on the camera. The processing of the raw PLIF images included corrections for background, camera sensitivity, and laser intensity profile.
Again, an additional ICCD camera was included in the setup for acquiring images of the OH* chemiluminescence giving important information about the size and the shape of the flame zone.

<Figure 3>

2.4. 1D laser Raman spectroscopy

A unique laser system designed at the DLR was used for the Raman experiments [12]. It consists of three double-pulse Nd:YAG lasers (Spectra-Physics PIV-400, frequency-doubled to 532 nm, 5 × 300 mJ pulse energy, one resonator out of operation, 7 ns pulse duration each). The five pulses are emitted with short delay times of about 50 ns nanoseconds between the single peaks. They pass a pulse stretching unit reducing the peak power of the pulse to a fifth of the original value while the complete pulse energy is nearly maintained. Because of the

naturally low quantum efficiency of the Raman scattering process, high laser pulse energies have to be used for single-shot measurements. If the peak power is not reduced, the high power density can either damage the combustor windows or produce an interfering plasma breakdown in the laser focus. The whole laser system is integrated in two temperature stabilized mobile containers enabling the application of the Raman technique at test rig facilities. The complete diagnostic setup is shown in Fig. 4.

<*Figure 4*>.

After an expansion of the laser beam to a diameter of about 40 mm, it passed through the focusing optics consisting of two cylindrical lenses which were oriented perpendicular towards each other. This astigmatic arrangement generated a stretched focus with a much lower energy density than a simple point-focus. Along the observed section of the laser beam the beam diameter was below 0.5 mm. The initial pulse power was reduced by several beam forming devices, the windows of the pressure vessel and impurities in the combustor windows. Therefore, the laser energy inside the combustion chamber never exceeded 890 mJ/pulse. After passing through the pressure vessel, the beam was collimated into the detector head of a power meter. The scattered light from the focus was collected at 90° with a large *f*/2 apochromatic lens system that relayed the focal region of the laser beam onto the entrance slit of a grating spectrograph (Acton Research SpectraPro 300i, f = 300 mm, 490 lines/mm, *f*/4, dispersion ~6 nm/mm). The magnification of the detection optics was 2. A holographic notch filter in front of the spectrograph blocked the Rayleigh scattered light and the stray light at 532 nm. The spectrally dispersed image of the beam was captured by a CCD chip (Princeton Instruments PI-Max, 1340 × 1300 pixels, 26.8 mm × 26 mm) equipped with an image intensifier. By applying a hardware binning of the pixel intensities it was possible to lower the effect of readout noise. In this way, the 1D measurement volume was divided into 28 cells each with a diameter of ~0.5 mm and 0.25 mm length. The 28 spectra from these cells were recorded simultaneously. In total 7 mm of the beam were used for probing the gas composition and temperature.
The whole diagnostic setup (except for the containers housing the laser system) was built on computer controlled 3D translation stages. This made it possible to scan a wide range of measurement locations. At some of the operating points up to 60 spatial locations were investigated. With a repetition rate of 10 Hz the concentrations of the major chemical species (CO_2, O_2, CO, N_2, C_xH_y, H_2O, H_2) were measured. Further important scalars such as the temperature and the mixture fraction can be derived from these values [26].
Extensive calibration measurements are indispensable for the correct analysis of the raw data. For this purpose, the setup was used to measure the temperature and the chemical composition of different electrically heated gas flows as well as flat laminar CH_4/air and H_2/air flames with known exhaust gas temperatures. These atmospheric calibration flames were provided by a custom-built matrix burner installed in the high-pressure test rig. The relative standard deviation of the single-shot temperature measurements in lean CH_4/air calibration flames was typically 8%. This value can be regarded as a rough assessment of the uncertainty of the temperature measurements at the gas turbine flames. More detailed specifications concerning the accuracy and the precision of the multiscalar measurements are currently in preparation.

3. Experimental results

3.1. Results from planar flow field measurements

Fig. 5 shows a vector plot of the average flow field together with the RMS fluctuations (in grey scales) for a flame at a pressure of p = 3 bar, a relative pressure drop over the burner of $\Delta p/p$ = 1 % and an equivalence ratio of Φ = 0.59. The burner mouth is on the left side, indicated by two marks.

<*Figure 5*>

The main characteristics of the mean flow field are a conically shaped region of the inflow with the highest flow velocities, an inner recirculation zone (IRZ) which extends back into the burner mouth and an outer recirculation zone (ORZ). The ORZ could not be imaged completely, because the outermost regions of the combustion chamber were vignetted by mechanical elements. Between the inflow and the recirculation zones, shear layers are established which can be recognized in the figure by the high RMS values. Another region of large RMS fluctuations is seen on the right hand side near the flame axis. This is probably caused by an exhaust gas swirl attached to the exit of the exhaust gas transition duct and reaching far upstream towards the burner. This assumption is supported by CFD simulations of the flow field in combustors with similar geometries [27, 28]. A slight deviation of the flow field from axial symmetry is visible near the flame axis. This is not really surprising because swirling flows are very sensitive even to very small deviations of the boundary conditions from axial symmetry, e.g. induced by the feed pipes or other mechanical parts. A remarkable feature of the flow field was observed by comparing the mean flow field for different operating conditions. The shape did not change by varying the system pressure, the mass flow or the equivalence ratio. This indicates that the averaged flow field (except of its absolute velocity values) is mainly dictated by the combustor geometry.
The instantaneous structures of the flow field were visualized by single-shot PIV measurements. Fig. 6 shows two examples from a series of measurements at identical operating conditions (p = 3 bar, $\Delta p/p$ = 1 %, Φ = 0.59). It is immediately seen that the instantaneous flow field looks totally different from the mean flow field and that strong temporal fluctuations of the structures occur. The instantaneous velocity field in the inner shear layer is dominated by small vortices which form and dissipate spontaneously. The observed vortex diameters range typically from 0.5 cm to 2 cm. The largest diameters are about 5 cm. Single shots of the PIV also show a varying backflow into the burner nozzle. While the backflow is relatively slow and undirected in Fig. 6 (a), two remarkable vortices in Fig. 6 (b) are located close to the burner mouth generating a massive backflow with planar velocities nearly as high as in the inflow region.

<*Figure 6*>

Complete vortices of the outer recirculation zone are rarely seen. This might indicate that the ORZ consists of only a few large vortices with their centers located close to the combustor side wall which can not be viewed due to the vignetting effect mentioned above.
Some of the instantaneous flow fields contain spots of high velocity located close to the combustor axis. Fig. 6 (b) shows an example on the right-hand side of the field of view. The intensity of this phenomenon is strongly varying and its location matches with the axial region of high RMS fluctuations described above. Thus, it is most likely caused by the rotating exhaust gas swirl.

3.2. Planar OH distribution

At chemical equilibrium, the concentration of OH radicals is exponentially dependent on the local temperature. With a typical OH PLIF system OH concentrations can be detected at temperatures above ≈1400 K in case of lean flames. The radicals are formed in super-equilibrium concentrations close to the flame front and the relaxation towards equilibrium is taking place within several milliseconds at atmospheric pressure [29]. Because the relaxation happens via three-body collisions, the decay time decreases rapidly with increasing pressure. Fig. 7 (a) shows a single shot of the LIF distribution at a relatively low pressure (p = 1.5 bar) and a low mass flow rate. The black regions represent the cold inflow of the unburnt fuel/air mixture. The regions with maximum LIF intensity seen in the shear layers are reflecting super-equilibrium concentration. The steep gradient from the dark inflow region to the fluorescence maximum is a good marker for the flame front [29]. The inner and the outer recirculation zones are characterized by medium and low LIF intensities with a more homogeneous distribution. This is typical of equilibrium OH concentrations indicating hot exhaust gas.

<Figure 7>

The instantaneous PLIF image exhibits corrugated flame fronts in the inner and outer shear layers. The lower LIF intensity seen in the lower part of the image is due to absorption of the laser light which is irradiated from the top to the bottom. In this single-shot exposure we see a large relatively homogeneous region of OH in the IRZ indicating gas at high temperature. An operating point with a higher pressure (p = 4 bar) and a higher mass flow was used to produce the single shot image of Fig. 7 (b). Here we clearly see an increased corrugation together with a fragmentation of the flame front. The isolated flame front fragments lead to the assumption of the occurrence of local flame extinction and spontaneous ignition. In contrast to the image at lower pressure, the shape of the regions with and without OH (IRZ and inflow) is subject to more fluctuations reflecting the higher degree of turbulence. By comparing the OH distributions of both shown operating conditions, it can be seen that maximum OH concentrations occur more frequently in the inner than in the outer shear layer, when the pressure is increased. This finding is consistent with the results of parameter studies investigating the OH* chemiluminescence distribution in the same combustor [23]. Although the OH PLIF measurements of this project do not provide quantitative results concerning the radical concentration, the high spatial resolution allows a statistical analysis of the fragmentation and the location of the flame front.

3.3. Mixture fraction and temperature statistics

The Raman technique enables the measurement of the instantaneous gas composition and therefore provides insight into the degree of mixing of fuel and air entering the combustion chamber. The scatter plot in Fig. 8 shows the result of such a measurement (p = 3 bar). It illustrates the correlation of the temperature T with the local mixture fraction ξ.

<Figure 8>

The spots represent the results obtained for each of the 28 measuring volumes along the laser line for a series of 500 single shot measurements. The blue spots in the plot indicate single shot results with H_2O concentrations below 1 vol.-‰, i.e. unburnt gas at inlet temperature. A significant variation of ξ is reflected by the broad distribution of the spots. This fluctuation exceeds the measurement uncertainty by far, and does not stem from an unstable mass flow of the fuel supply of the test rig. Therefore, the variation of ξ reflects the degree of mixing of

fuel and air. The equivalence ratio ranges from lean mixtures with fuel concentrations below the ignition limit to nearly stoichiometric mixtures. It is known that a perfect mixing is impossible to achieve under industrial conditions because of the short residence time in the premix region. However, the degree of mixing of fuel and air plays an important role for the combustion behavior, for example for the flame stabilization and NO_x formation. The quality of the mixing and its spatial and temporal fluctuations can hardly be measured quantitatively by methods other than Raman scattering, and this is the first time the level of unmixedness was directly determined for an industrial GT burner.
Our Raman measurements also show how the hot reaction products mix with the reactants in the shear layer of the flow. The scatter plot in Fig. 9 was recorded with the measuring volume located inside the inner shear layer a few centimeters downstream of the burner mouth. Again, blue spots represent the non-reacted fuel/air mixture, whereas the red spots indicate single shot results with less than 1 vol.-‰ of natural gas corresponding to the hot reaction products. It is clearly seen, that reactants as well as products are present in the inner shear layer. In some single shots both compositions are present next to each other at the same time. In that case some of the CCD pixel rows show spectra of cold fuel and air while the others detect hot exhaust gas. Some of these single shots were possibly recorded at a point of time when the laser beam was penetrating the flame front.

<Figure 9>

The green curve displayed in the scatter plots indicates the adiabatic flame temperature calculated with the program Gaseq [30]. As can be seen, some of the single shot measurements exhibit temperatures above the adiabatic temperature. This discrepancy is mainly due to the uncertainty of the diagnostic method. Possible pressure fluctuations and the shot noise of the detected photons are two examples for phenomena leading to an increased standard deviation of the statistical distribution of the scalar values. Additionally, some processes are conceivable that may in fact cause super-equilibrium temperatures, e.g. temperature increase of unburned gas by contact to hot surfaces prior to combustion. The black spots in the figure represent single shots with intermediate temperatures and chemical compositions of burnt and unburnt gas. At least three processes can theoretically lead to such distributions:

- Events of local flame extinction caused by a high strain rate of the flow interrupt the chemical reaction before all of the fuel is consumed. Though local flame extinction does certainly occur it is not likely that this scenario happens frequently enough to explain the observed high density of intermediate points.
- Spatial averaging across the flame front: If the laser is passing through a flame front, gradients of temperature and composition may be present in one single observation volume or across several observation volumes, depending on the angle of intersection.
- The mixing of exhaust gas with unburnt fuel and air may instantaneously generate regions within the shear layer where reactants and products are completely mixed. This kind of mixture seems to be captured by the Raman system before it ignites spontaneously or by flame propagation.

Because of the short turbulent mixing time scale in such flows, a large portion of the intermediate points in the scatter plot is most likely formed by the third process where mixtures formed from the fresh fuel/air and exhaust gases did not react completely due to their ignition delay time.

4. Summary and Conclusions

Several laser optical diagnostic methods have been used to study lean premixed natural gas/air flames of an industrial swirl burner at elevated pressures. For this purpose the burner was equipped with an optical combustion chamber and installed at the high pressure test rig facility in Stuttgart. The burner was operated at gas turbine relevant conditions with preheated air, high thermal power and a lean air/fuel ratio. The flow velocities were measured by particle image velocimetry (PIV), the flame structures by planar laser induced fluorescence (PLIF) of OH and the joint probability density functions (PDFs) of the major species concentrations, mixture fraction and temperature by 1D laser Raman scattering.
The averaged flow field can be divided into three main regimes: The conically shaped inflow region, the large inner recirculation zone and the outer recirculation zone. Parameter studies proved that the spatial structure of these three regions was not influenced by the operating conditions. By analyzing the PIV single shots it was seen that the instantaneous structure of the IRZ consisted of several small vortices mainly located inside the inner shear layer. According to this, the standard deviation of the flow velocity indicated a high level of turbulence in the shear layers. RMS mappings of the velocity also revealed the existence of an exhaust gas swirl.
Instantaneous planar LIF measurements of OH revealed wrinkled flame fronts between the inflow and the recirculation zones. Fragmentation and corrugation of the flame front increased when the Reynolds number of the flow was increased.
The multiscalar measurements provided by 1D laser Raman spectroscopy yielded the major species and temperature distributions for different flame conditions. They were used to determine the composition of the unburnt fuel/air mixture indicating a significant variation of the local equivalence ratio. For the first time it was possible to quantify the degree of unmixedness in an industrial GT combustor under realistic operating conditions. Raman measurements at locations inside the inner shear layer revealed a large variation of the thermo-chemical state of the flame, reaching from non-reacted via partially reacted to completely reacted. The intermediate partially reacted mixtures are probably to be explained as mixing of hot reaction products with the fresh fuel/air mixture which have not reacted yet due to ignition delay.
In conclusion, the experimental data base provides a better understanding of the interaction between turbulent flow and chemical processes and will be useful for the validation and the improvement of numerical flame simulations. Future work will be carried out by the German Aerospace Center (DLR) in cooperation with Siemens Industrial Turbomachinery Ltd. in order to further develop modeling capabilities and design tools for commercial gas turbine combustors.

Acknowledgment

The presented work was conducted at the German Aerospace Center (DLR) in cooperation with SIEMENS Industrial Turbomachinery. We gratefully acknowledge the financial support from the State of Baden-Württemberg within the KW21 research program.

References

[1] C.O. Paschereit, E. Gutmark, W. Weisenstein, Structure and Control of Thermoacoustic Instabilities in a Gas-Turbine Combustor, Combust. Sci. Technol. 138 (1998) 213-232.
[2] A.H. Lefebvre, Gas Turbine Combustion, Taylor & Francis, Philadelphia, 1999.

[3] J.G. Lee, D.A. Santavicca, Experimental Diagnostics for the Study of Combustion Instabilities in Lean Premixed Combustors, J. Propulsion and Power 19 (2003) 735-750.
[4] T. Sattelmayer, Influence of the Combustor Aerodynamics on Combustion Instabilities from Equivalence Ratio Fluctuations, J. Eng. Gas Turbines Power 125 (2003) 11-19.
[5] T.C. Lieuwen, V. Yang, Combustion Instabilities in Gas Turbine Engines: Operational Experience, Fundamental Mechanisms, and Modeling, Progr. Astronaut. Aeronaut. 210 (2006).
[6] K.J. Syed, E. Buchanan, The Nature of NOx Formation within an Industrial Gas Turbine Dry Low Emission Combustor, Proc. ASME Turbo Expo 2005, Reno-Tahoe, Nevada, USA, June 6-9 2005, paper GT-2005-68070.
[7] W. Meier, P. Weigand, X.R. Duan, R. Giezendanner-Thoben, Detailed Characterization of the Dynamics of Thermoacoustic Pulsations in a Lean Premixed Swirl Flame, Combust. Flame 150 (2007) 2-26.
[8] X.R. Duan, W. Meier, P. Weigand, O. Keck, B. Lehmann, W. Stricker, M. Aigner, Experimnetal investigation and laser based validation measurements in a gas turbine model combustor, Prog. Comp. Fluid Dynamics 4 (2004) 175-182.
[9] N. Syred, A Review of Oscillation Mechanisms and the Role of Precessing Vortex Core (PVC) in Swirl Combustion Systems, Prog. Energy Combust. Sci. 32 (2006) 93-161.
[10] M. Stöhr, R. Sadanandan, W. Meier, Experimental study of unsteady flame structures of an oscillating swirl flame in a gas turbine model combustor, Proc. Comb. Inst. 32 (2009) 2925-2932.
[11] W.A. Guttenfelder, M.W. Renfro, N.M. Laurendeau, J. Ji, G.B. Galen, J.P. Gore, Hydroxyl Time-Series and Recirculation in Turbulent Nonpremixed Swirling Flames, Combust. Flame 147 (2006) 11-21.
[12] L. Wehr, W. Meier, P. Kutne, C. Hassa, Single-pulse 1D laser Raman scattering applied in a gas turbine model combustor at elevated pressure, Proc. Comb. Inst. 31 (2007) 3099-3106.
[13] W. Meier, X.R. Duan, P. Weigand, Investigations of Swirl Flames in a Gas Turbine Model Combustor. Part II: Turbulence-Chemistry Interactions, Combust. Flame 144 (2006) 225-236.
[14] R.S. Barlow, Laser diagnostics and their interplay with computations to understand turbulent combustion, Proc. Comb. Inst. 31 (2007) 49-75.
[15] S.-Y. Lee, S. Seo, J.C. Broda, S. Pal, R.J. Santoro, An Experimental estimation of Mean Reaction Rate and Flame Structure during Combustion Instability in a Lean Premixed Gas Turbine Combustor, Proc. Combust. Inst. 28 (2000) 775-782.
[16] U.E. Meier, D. Wolff-Gaßmann, W. Stricker, LIF Imaging and 2D Temperature Mapping in a Model Combustor at Elevated Pressure, Aerosp. Sci. Technol. 4 (2000) 403-414.
[17] C. Löfström, J. Engström, M. Richter, C.F. Kaminski, P. Johansson, K. Nyholm, J. Nygren, M. Aldén, Feasibility Studies and Application of Laser/Optical Diagnostics for Characterisation of a Practical Low-Emission Gas Turbine Combustor, Proc. ASME Turbo Expo 2000, Munich, Germany, May 8-11 2000, paper 2000-GT-0124.
[18] J.R. Gord, M.S. Brown, T.R. Meyer, Optical Diagnostics for Characterizing Advanced Combustors and Pulsed-Detonation Engines, 22nd AIAA Aerodynamic Measurement Technology and Ground Testing Conference, St. Louis, Missouri, USA, 24-26 June 2002, paper AIAA2002-3030.
[19] J. Kojima, Q.-V. Nguyen, Measurement and Simulation of Spontaneous Raman Scattering in High-Pressure Fuel-Rich H_2-Air Flames, Meas. Sci. Technol. 15 (2004) 565-580.

[20] C. Willert, C. Hassa, G. Stockhausen, M. Jarius, M. Voges, J. Klinner, Combines PIV and DGV applied to a pressurized gas turbine combustor facility, Meas. Sci. Technol. 17 (2006) 1670-1679.
[21] P. Griebel, P. Siewert, P. Jansohn, Flame characteristics of turbulent lean premixed methane/air flames at high pressure: Turbulent flame speed and flame brush thickness, Proc. Combust. Inst. 31 (2007) 3083-3090.
[22] B. Janus, A. Dreizler, J. Janickam, Experiments on swirl-stabilized non-premixed natural gas flames in a model gasturbine combustor, Proc. Comb. Inst. 31 (2007) 3091-3098.
[23] U. Stopper, M. Aigner, W. Meier, R. Sadanandan, M. Stöhr, I.S. Kim, Flow Field and Combustion Characterization of Premixed Gas Turbine Flames by Planar Laser Techniques, J. Eng. Gas Turb. Power 131 (2009) 21504.
[24] P.A. Strakey, S.D. Woodruff, T.C. Williams, R.W. Schefer, OH-Planar Fluorescence Measurements of Pressurized, Hydrogen Premixed Flames in the SimVal Combustor, AIAA J. 46 (2008) 1604-1613.
[25] W. Ng, K. Syed, Y. Zhang, The Study of Flame Dynamics and Structures in an Industrial-Scale Gas Turbine Combustor Using Digital Data Processing and Computer Vision Techniques, Meas. Sci. Technol. 15 (2004) 2303-2309.
[26] R.W. Bilger, The Structure of Turbulent Nonpremixed Flames, Proc. Combust. Inst. 22 (1988) 475-488.
[27] M.D. Turrell, P.J. Stopford, K.J. Syed, E. Buchanan, CFD Simulation of the Flow Within and Downstream of a High-Swirl Lean Premixed Gas Turbine Combustor, Proc. ASME Turbo Expo 2004, Vienna, Austria, June 14-17 2004, paper GT-2004-53112.
[28] T.C. Williams, R.W. Schefer, J.C. Oefelein, C.R. Shaddix, Idealized gas turbine combustor for performance research and validation of large eddy simulations, Rev. Sci. Instrum. 78 (2007) 035114.
[29] R. Sadanandan, M. Stöhr, W. Meier, Simultaneous OH-PLIF and PIV measurements in a gas turbine model combustor, Appl. Phys. B 90 (2008) 609-618.
[30] C. Morley, Gaseq, A Chemical Equilibrium Program for Windows, URL: http://www.gaseq.co.uk (2009).

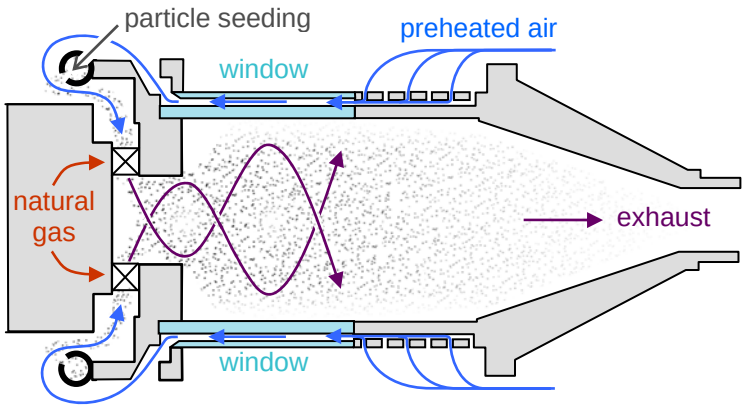

Fig. 1. The optical combustor with particles seeded into the air upstream of the swirler.

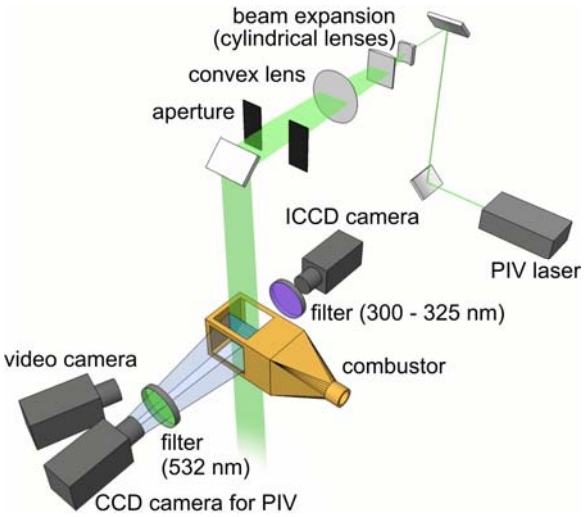

Fig. 2. Experimental setup for particle image velocimetry. The video camera was used for controlling purposes only.

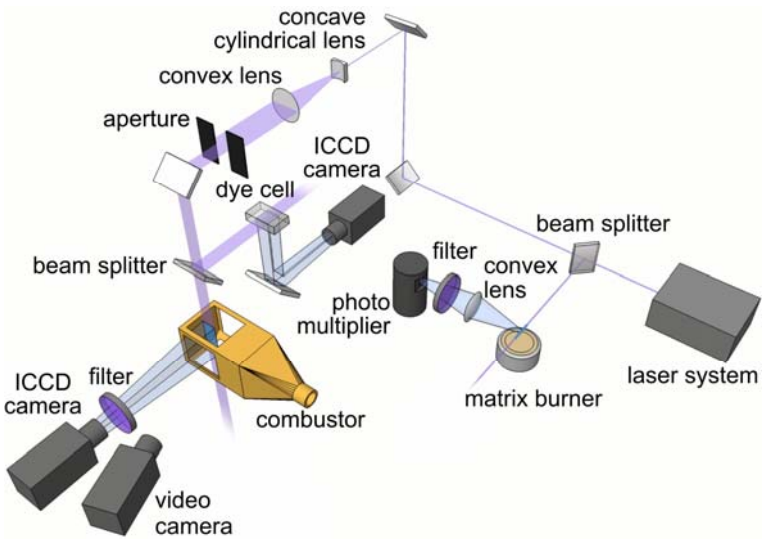

Fig. 3. Experimental setup for the PLIF imaging. The video camera was used for controlling purposes only.

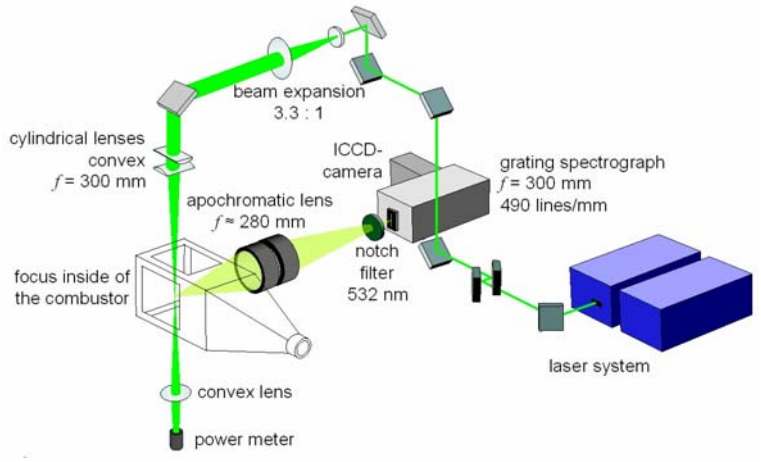

Fig. 4. Experimental setup for 1D laser Raman spectroscopy.

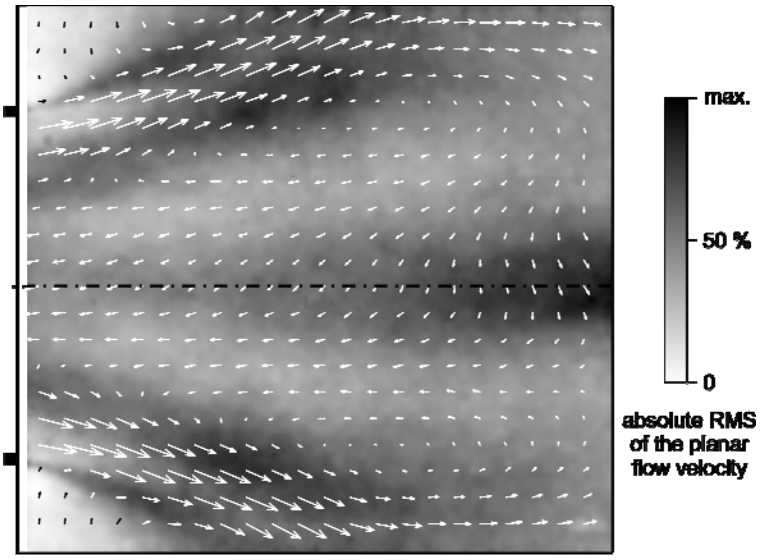

Fig. 5. Background: Mapping of the absolute standard deviation of the planar flow velocity. Overlay: Vector array of the average planar flow field.

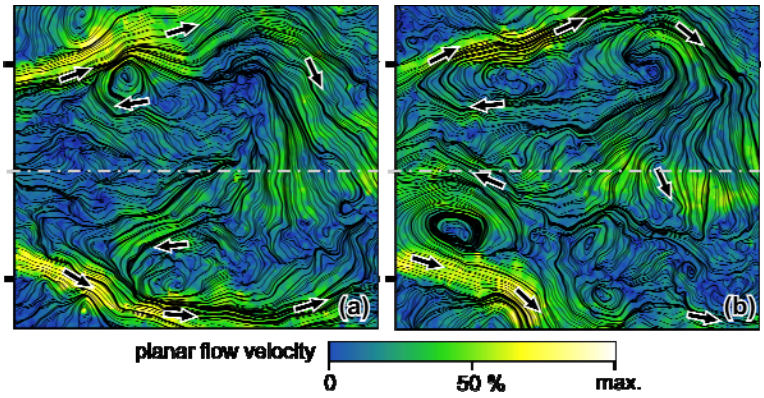

Fig. 6. Two examples of streamline plots of the instantaneous flow field measured at the same operating point. Arrows indicate the local flow direction. The pair of marks drawn on the left side of each image indicates the diameter of the burner exit.

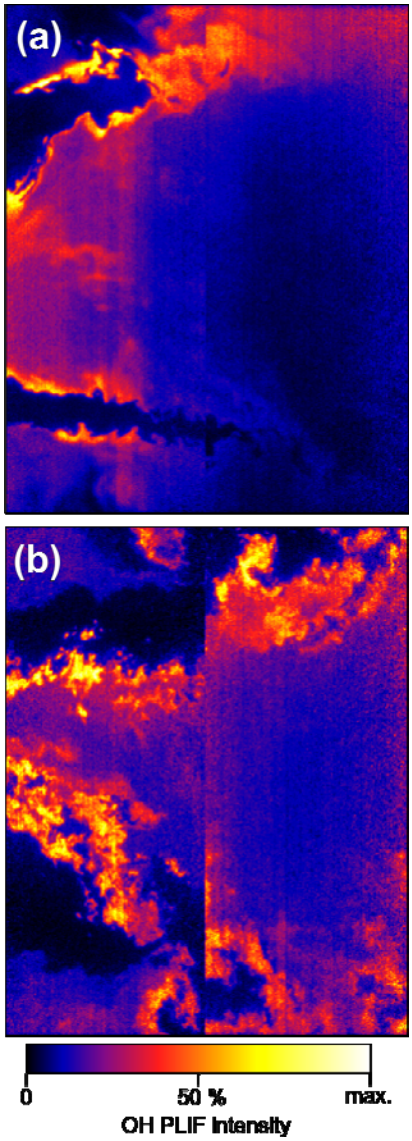

Fig. 7. PLIF images showing the instantaneous distribution of OH radicals for two operating conditions: (a) p = 1.5 bar, $\Delta p/p$ = 1.1%, Φ = 0.53; (b) p = 4 bar, $\Delta p/p$ = 3%, Φ = 0.50. Each figure is a composite of two different laser sheet positions imaged at different points in time.

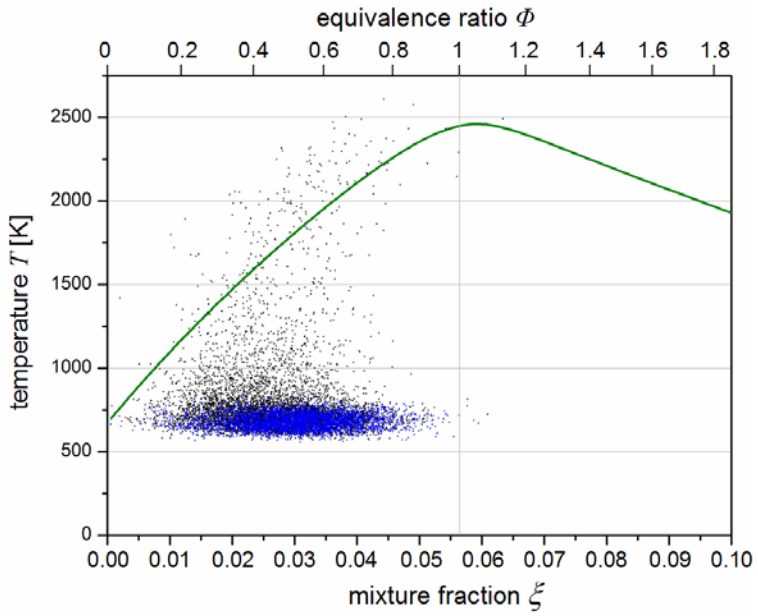

Fig. 8. Scatter plot (14,000 points) of the temperature and the mixture fraction measured in the inflow of the unburnt fuel/air mixture. Blue points: $X_{H2O} \approx 0$. The green curve represents the calculated adiabatic temperature of the reaction products.

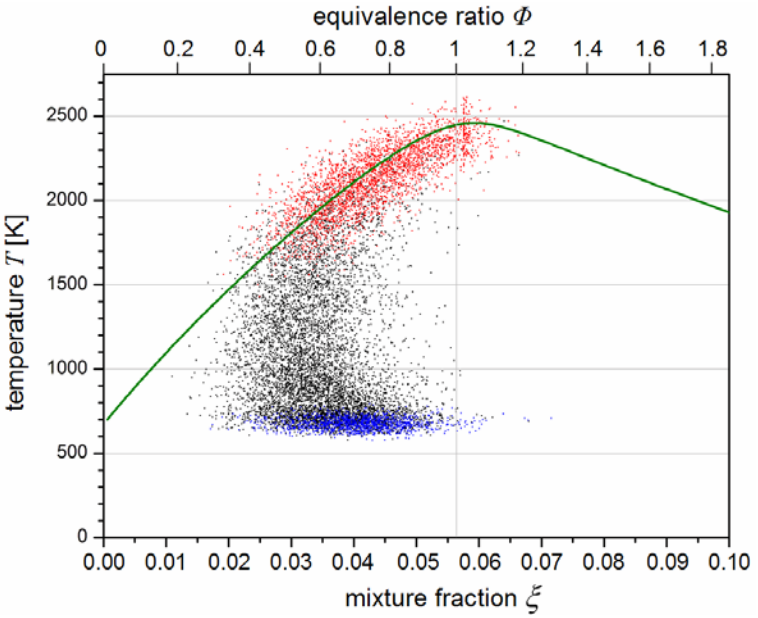

Fig. 9. Scatter plot (14,000 points) of the temperature and the mixture fraction measured in the inner shear layer. Blue points: $X_{H2O} \approx 0$. Red points: $X_{fuel} \approx 0$. The green curve represents the calculated adiabatic temperature of the reaction products.